Science Advances
AAAS

Supplementary Materials for

TERT accelerates BRAF mutant–induced thyroid cancer dedifferentiation and progression by regulating ribosome biogenesis

Pengcheng Yu *et al.*

Corresponding author: Yu-Long Wang, yulongwang@fudan.edu.cn; Fa-Xing Yu, fxyu@fudan.edu.cn

Sci. Adv. **9**, eadg7125 (2023)
DOI: 10.1126/sciadv.adg7125

The PDF file includes:

Figs. S1 to S9
Legends for tables S1 to S4

terial for this manuscript includes the following:

Tables S1 to S4

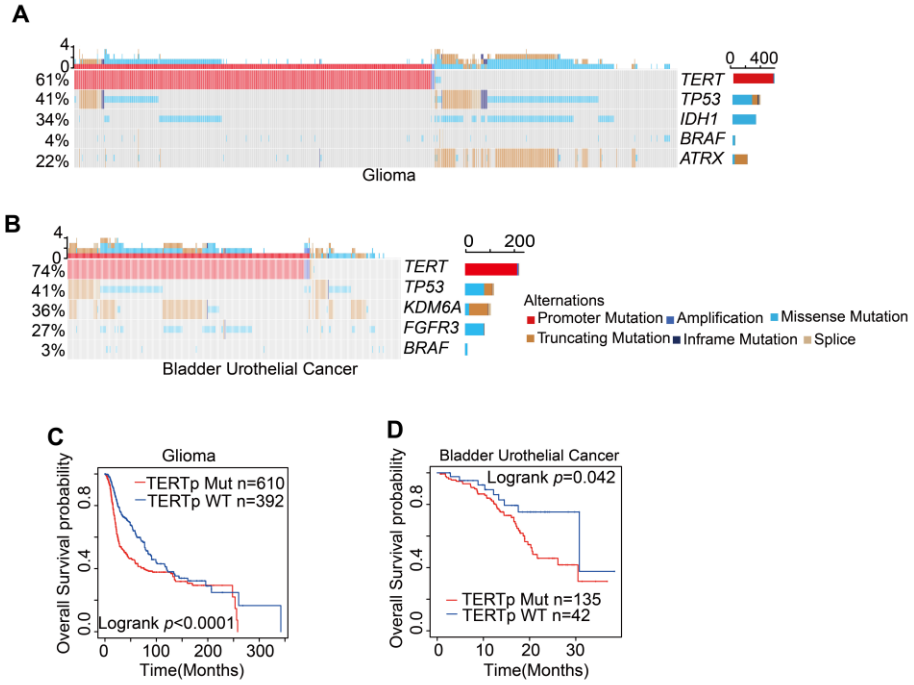

Figure S1. *TERT* promoter mutation occurs frequently in cancers and predicts a worse prognosis.

A. and B. Mutation landscape of glioma and bladder urothelial cancer.

C. and D. Comparison of survival curves based on *TERT* promoter status in glioma and bladder urothelial cancer.

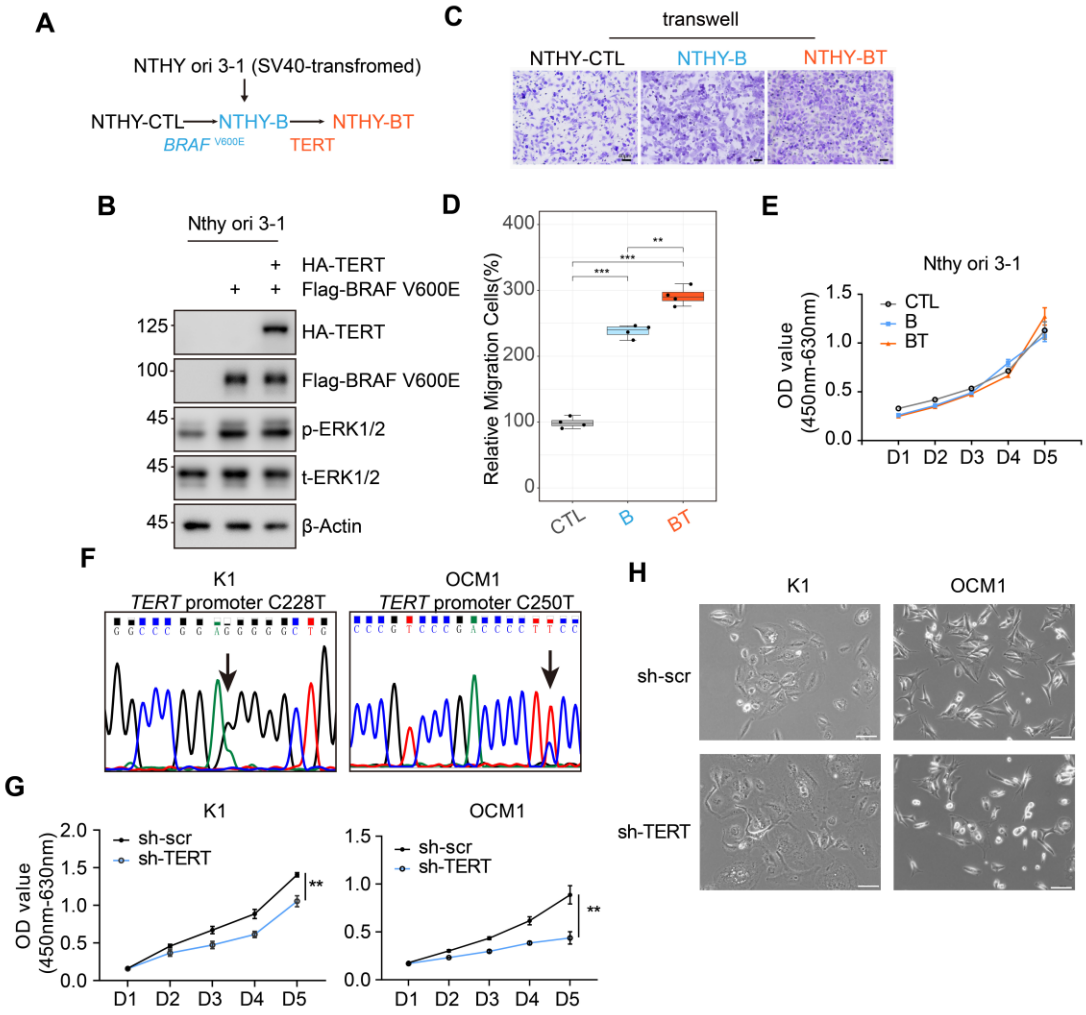

Figure S2. TERT partly regulates tumor cell migration and proliferation *in vitro*.

A. Schematic diagram of stable transfected NTHY ori 3-1 cell lines construction.

B. Western blot validation of NTHY-CTL, NTHY-B, and NTHY-BT cells.

C. and D. Photomicrographs and statistic results of transwell migration assays of the NTHY-CTL, NTHY-B, and NTHY-BT cells. Scale bar, 40 μm. Boxplot showed the median with IQR and 1.5 IQR whiskers. **, $p < 0.01$, ***, $p < 0.001$.

E. CCK8 assay shows that NTHY-CTL, NTHY-B, and NTHY-BT cells proliferated at a similar rate.

F. Sanger sequencing shows K1 and OCM1 separately have *TERT* promoter C228T or C250T mutation. Arrow, mutation site.

G. CCK8 assays show that TERT knockdown inhibits K1 and OCM1 proliferation. **, $p < 0.01$.

H. Bright field images of K1 and OCM1 cells stable infection with sh-scr or sh-TERT virus. Scale bar, 100 μm.

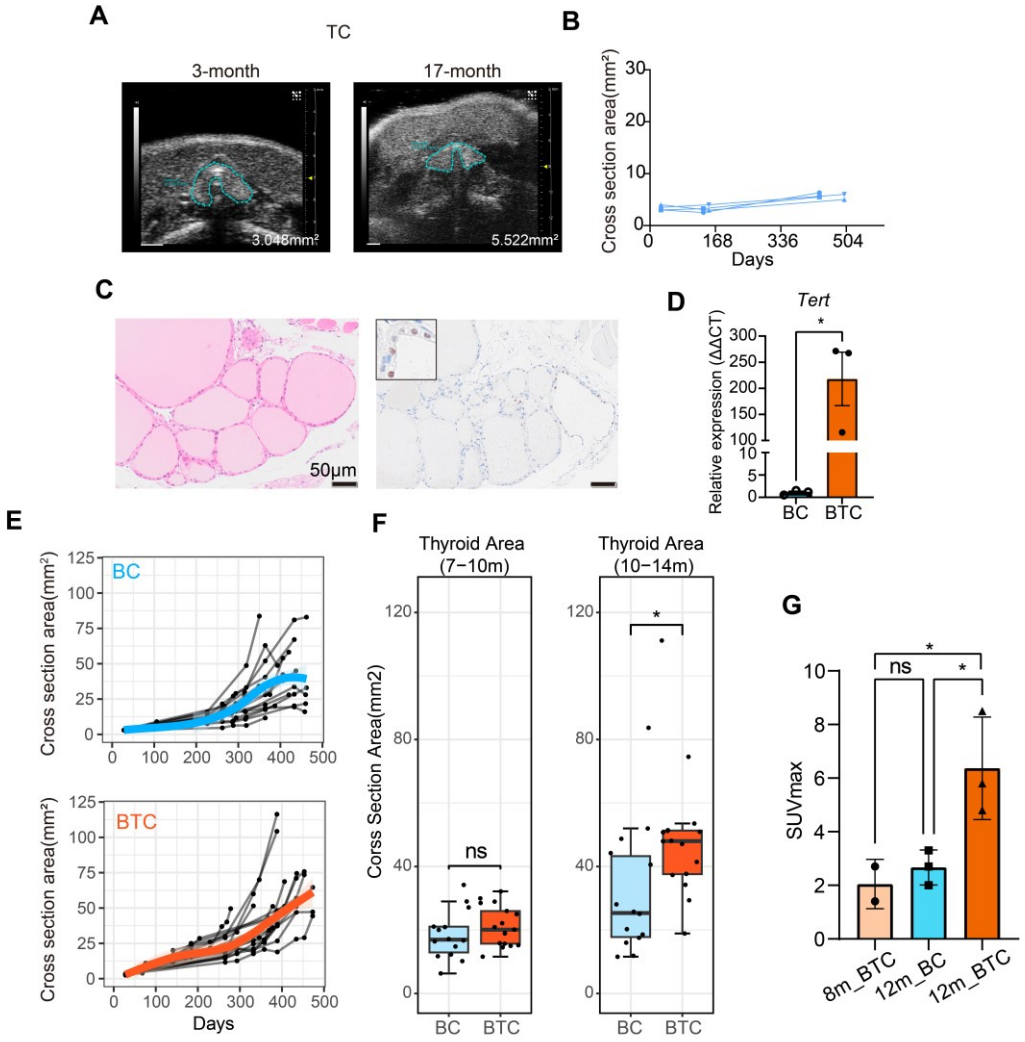

Figure S3. TERT alone fails to initiate tumor formation but accelerates *BRAF* V600E tumor growth.

A. Representative ultrasound imaging of TC mice thyroid at 3-month and 17-month old. Scale bar, 1 mm.

B. Growth patterns of TC mice thyroid (n=4).

C. H&E and anti-Flag IHC result of 17-month TC mice thyroid (scale bar, 50 μm).

D. The qPCR results of *Tert* mRNA expression levels in BC and BTC mouse thyroid glands.

E. Growth patterns of BC (n=14) and BTC (n=17) thyroid tumors.

F. Cross section area (mm^2) comparison of BC and BTC thyroid at 7-10m old or 10-14m old. Student's t-test. Boxplot shows the median with IQR and 1.5 IQR whiskers.

G. SUVmax values for PET-CT of 8m_BTC (n=2), 12m_BC (n=3) and 12m_BTC (n=3) thyroid. Data presented as mean±SD. One-way ANOVA and Tukey's multiple comparisons test. *, $p<0.05$.

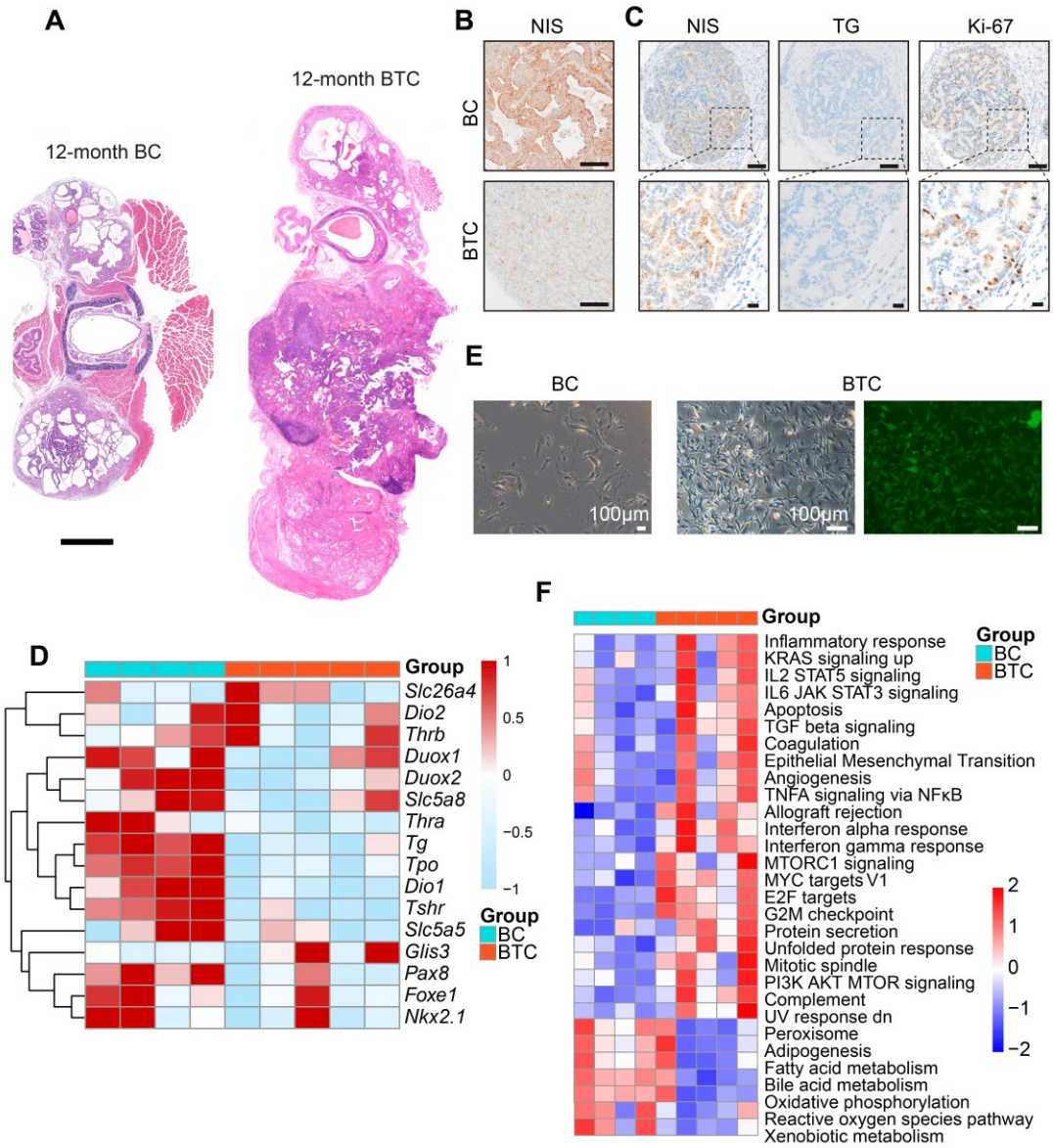

Figure S4. TERT promotes dedifferentiation of BRAF-induced thyroid cancer

A. Representative images of HE staining for the thyroid glands of 12-month-old BC and BTC mice. Scale bar = 1 mm.

B. NIS IHC results (scale bar, 100 μm) of BC and BTC mice thyroid.

C. NIS, TG, and Ki-67 IHC results of BTC mice lung metastasis foci (scale bar, up 100 μm; down 20 μm).

D. Heatmap shows the TDS genes expression in BC and BTC thyroid.

E. Morphology of primary thyroid cells derived from BC and BTC thyroid in bright and fluorescence field. Scale bar, 100 μm.

F. Heatmap shows Hallmarks GSVA results of BC and BTC mice thyroid.

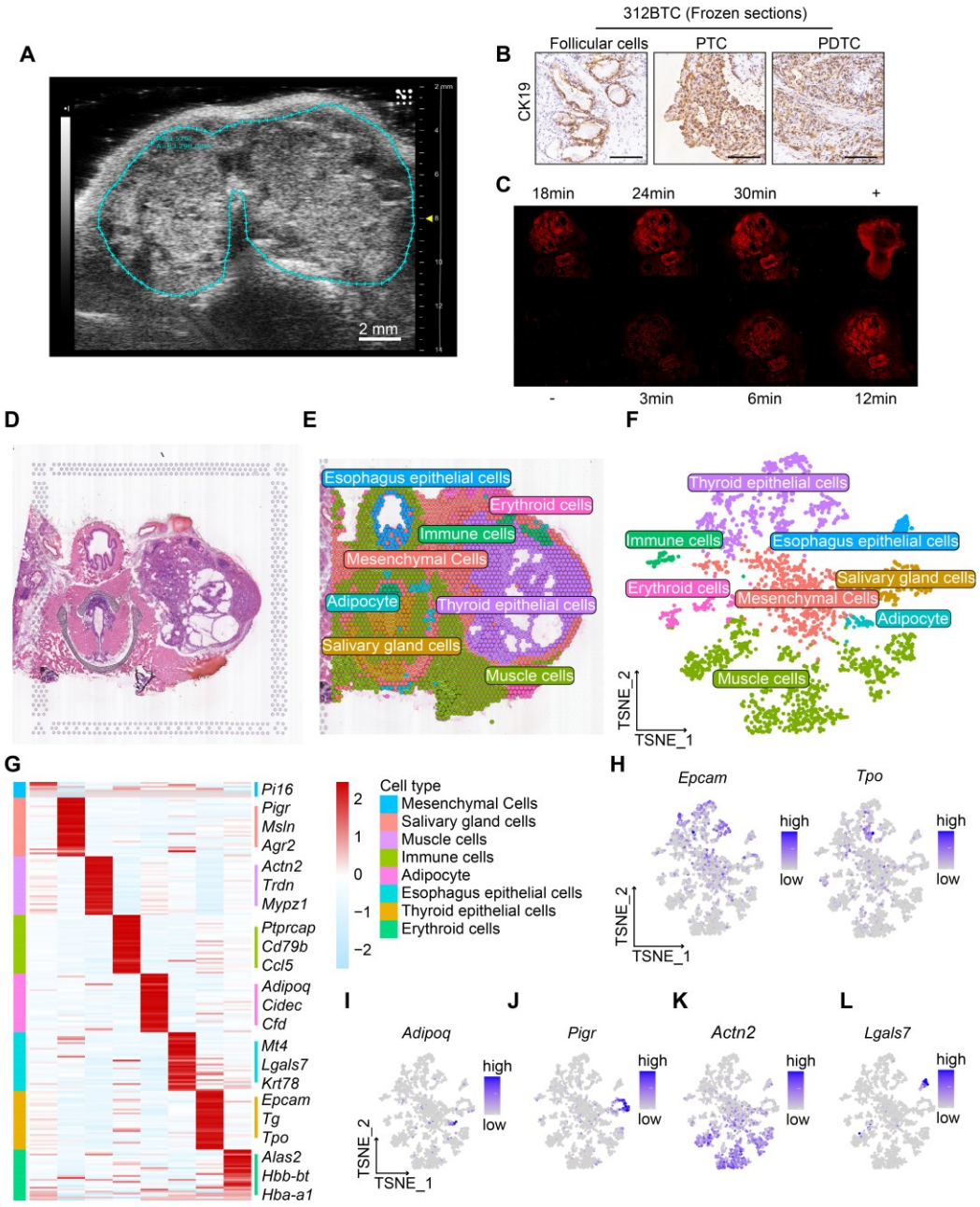

Figure S5. Identification of various components in 312BTC spatial transcriptome sample.

A. Ultrasound imaging of 312BTC thyroid. Blue dashed line region, thyroid tumor.

B. Anti-CK19 IHC staining of 312BTC thyroid. Scale bar, 100 μm.

C. Optimal permeabilization time for 312BTC thyroid.

D. H&E staining of 312BTC for 10X sequencing.

E. and F. Spatial and T-SNE projections show different cell types of all 312BTC spots.

G. Heatmap shows the relative expression levels of representative markers of different cell types.

H. I. J. K. and L. TSNE feature plots show the representative markers of the thyroid (*Epcam, Tpo*), adipocyte (*Adipoq*), salivary gland cells (*Pigr*), muscle cells (*Actn2*) and esophagus epithelial cells (*Lgals7*).

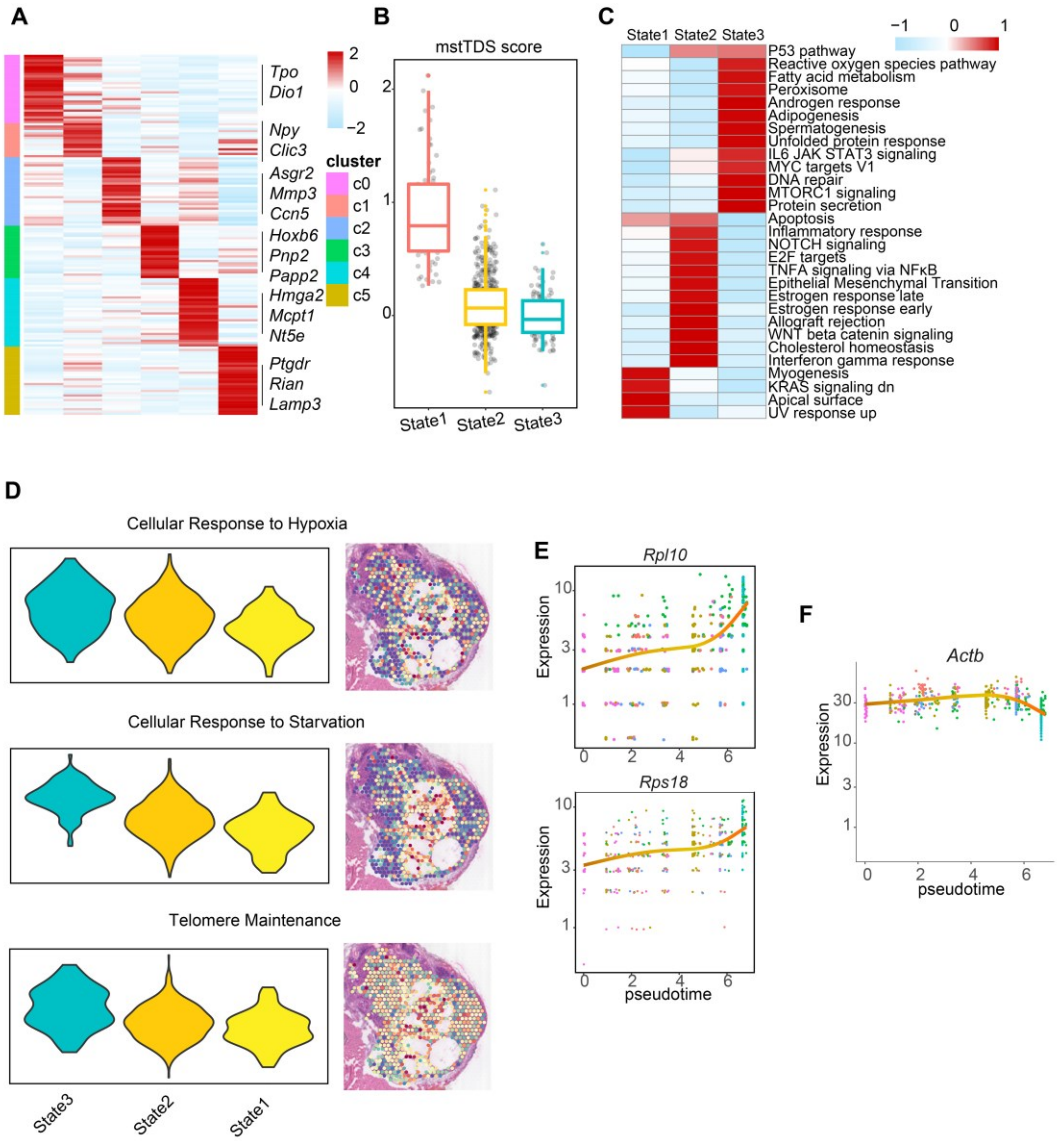

Figure S6. Characterization of different states of thyroid components of the spatial transcriptome.

A. Heatmap shows representative markers of six thyroid clusters.

B. Boxplot shows the decreasing trend of TDS score from state1 to state3.

C. Heatmap presents the GSVA enrichment scores of hallmark gene sets.

D. Violin plots and spatial plots show the activation of cellular response to hypoxia and starvation and telomere maintenance pathways in state 1/2/3 thyroid components.

E. F. Scatter plots show *Rpl10*, *Rps18,* and *Actb* gene expression level change over pseudotime, colored by clusters.

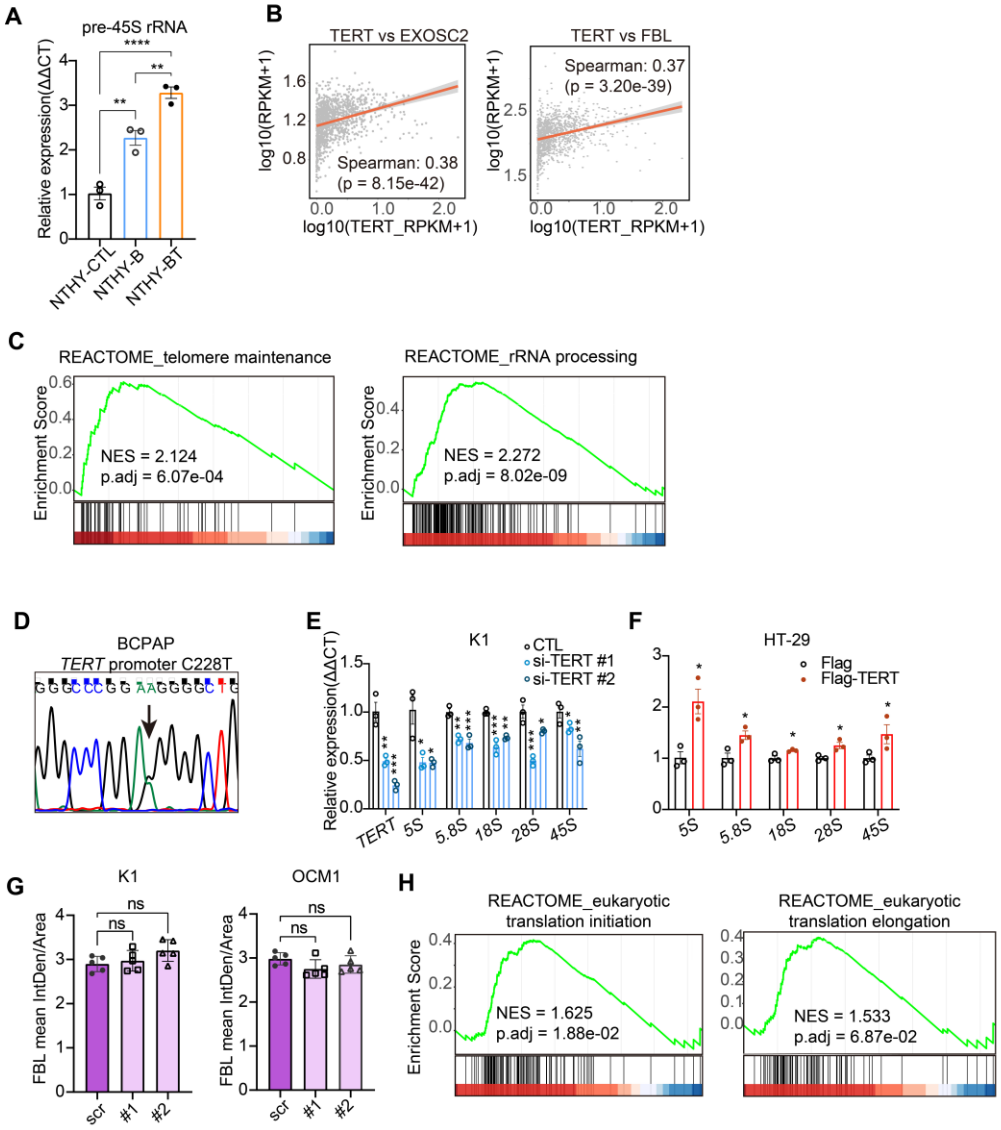

Figure S7. TERT regulates ribosome-related functions.

A. QPCR results of pre-45S rRNA in NTHY-CTL, NTHY-B, and NTHY-BT cells. Data presented as mean±SEM (n=3). **, p<0.01; ****, p<0.0001.

B. Correlation between TERT and EXOSC2, and FBL (n=1156).

C. GSEA results show TERT high-expression cells are positively enriched in telomere maintenance and RRNA metabolic process in the CCLE dataset.

D. Sanger sequencing result shows *TERT* promoter C228T mutation site in BCPAP.

E. and F. QPCR results of ribosomal RNA 5S, 5.8S, 18S, 28S, and 45S change after TERT knockdown (D, in K1 cells) and TERT over-expression (E, in HT-29 cells). Data presented as mean ±SD (n=5). *, p<0.05; **, p<0.01; ***, p<0.001.

G. Quantification results of fig.4F and fig.4H FBL fluorescence intensity using ImageJ software (n=5).

H. GSEA results show TERT high-expression cells are positively enriched in translation initiation and translation elongation.

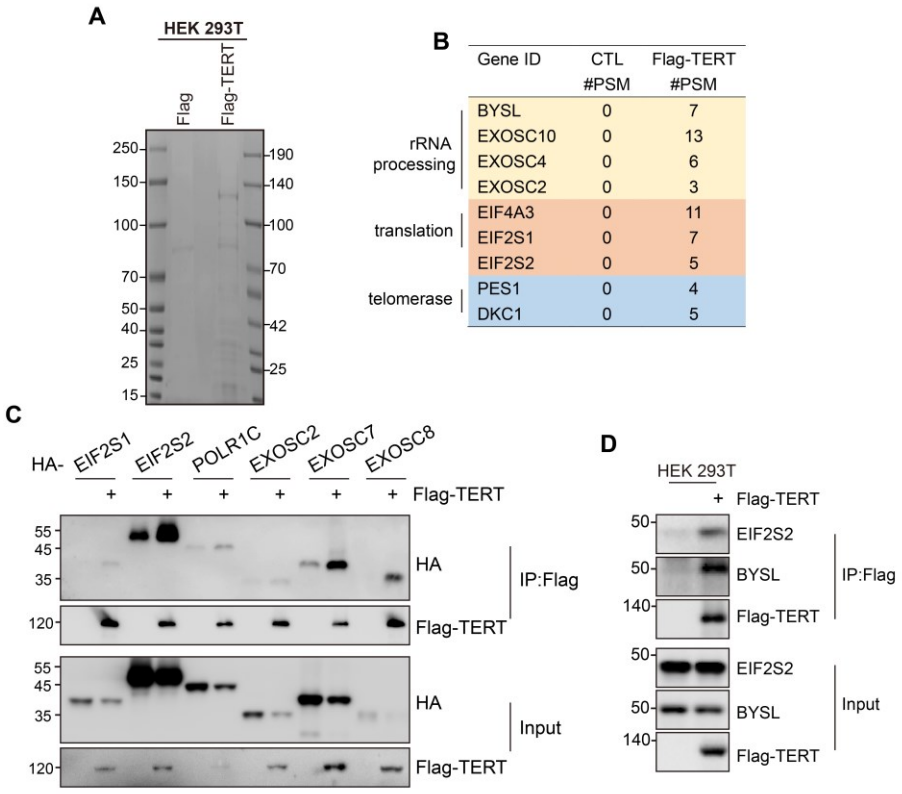

Figure S8. Identification of TERT-interacting proteins

A. SDS-PAGE of lysate immunoprecipitated with anti-Flag antibody shows the staining result of coomassie brilliant blue and rendered in grayscale.

B. Representative proteins identified by IP/LC-MS. PSM, peptide spectra match.

C. and **D.** Co-IP analysis of protein extracted from HEK 293T cells.

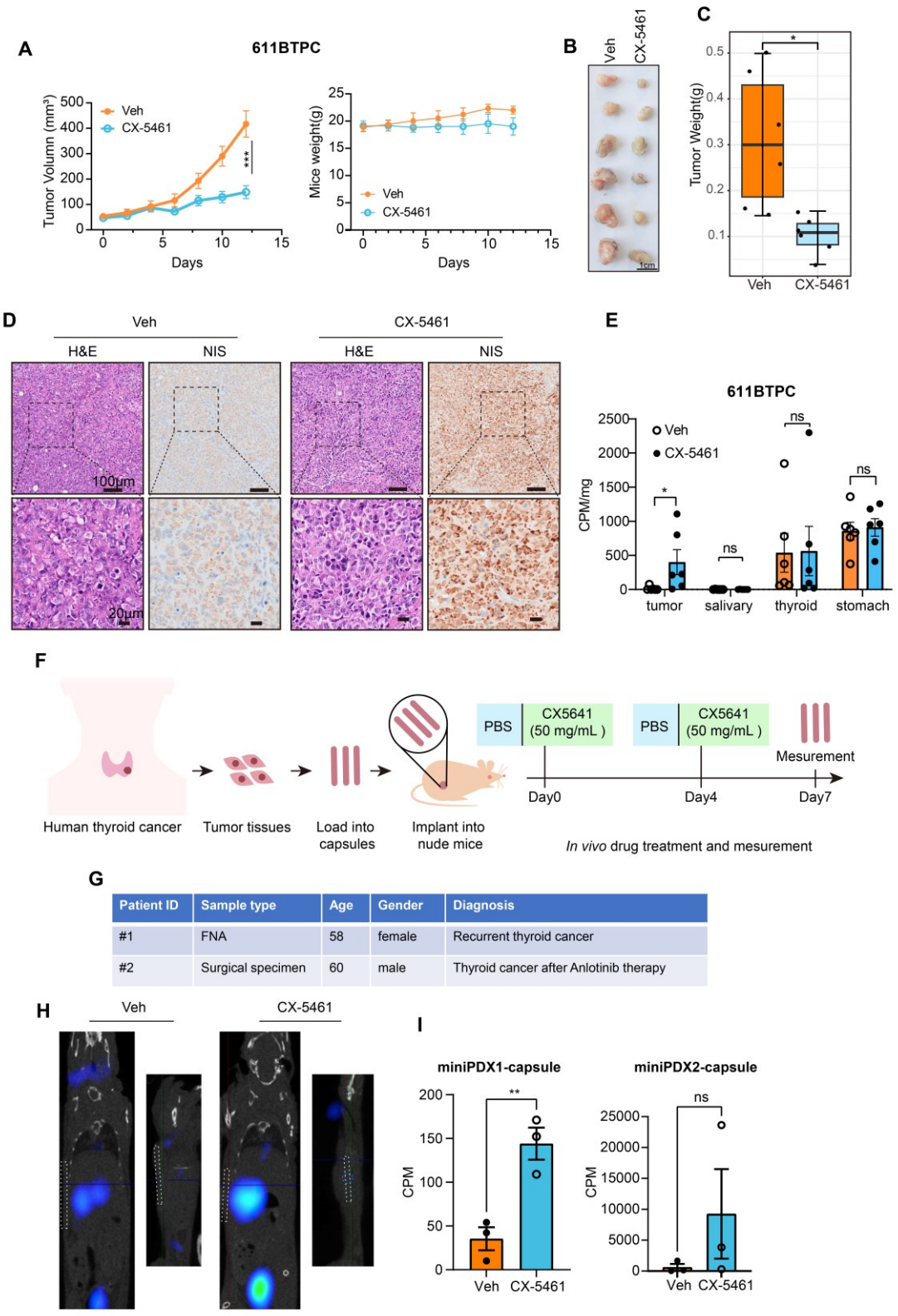

Patient ID	Sample type	Age	Gender	Diagnosis
#1	FNA	58	female	Recurrent thyroid cancer
#2	Surgical specimen	60	male	Thyroid cancer after Anlotinib therapy

Figure S9. CX-5461 inhibits tumor progression and induces thyroid cancer re-differentiation.
A. B. C. Growth curve, mice weight, tumor gross appearance and tumor weight of 611BTPC allografts treated by vehicle or CX-5461. n=6 for each group. P. O. for 4 times.
D. H&E morphology and anti-NIS staining after 5 times CX-5461 treatment in BCPAP xenografts.

E. Biodistribution of [^{125}I] in the tumor, salivary gland, thyroid and stomach of 611BTPC allografts. CPM, Counts Per Minute. Mann-Whitney test.

F. Schematic diagram of miniPDX of thyroid cancer.

G. Patient information for miniPDX tissue sources

H. Representative [^{125}I] imaging of miniPDX administrated with vehicle and CX-5461. The white and blue dash lines separately represent the subcutaneous capsule and the uptake signal at the capsule site.

I. Counts Per Minute (CPM) values of miniPDX capsules, normalized by cell viability. Data presented as mean±SEM.

Supplementary tables:

Table S1: Primers and DNA/RNA sequences.

Table S2: Antibodies list.

Table S3: Flag-TERT IP-MS results in HEK 293T.

Table S4: Bulk RNA-seq counts of BC (n=4) and BTC (n=5) thyroid.